Ammonia Room Temperature Gas Sensor Using Different TiO2 Nano-structure

Mostafa Shooshtari (m.shooshtari@tudelft.nl)
KNTU: KN Toosi University of Technology https://orcid.org/0000-0003-1292-0683
Alireza Salehi
K N Toosi University of Technology Faculty of Electrical Engineering

Research Article

Keywords: Gas sensor, titanium dioxide (TiO2), Nano-structure, ammonia sensor, nanowire, nanoparticle, thin-film

DOI: https://doi.org/10.21203/rs.3.rs-341152/v1

Abstract

In this study, TiO_2 Nano-structure were synthesized by three different processes including nanowires, nanoparticles and thin- films. The morphology and crystal structure of the three different TiO_2 structures deposited on quartz glasses were characterized by XRD, SEM and FTIR. It has been found that nanowires and nanoparticles showed only the anatase phase while the thin-film exhibited both anatase and rutile phases. The three TiO_2 Nano-structures were then used to fabricate gas sensors for ammonia (NH_3) detection at different concentrations and various conditions. The samples fabricated with thin-film TiO_2 towards 50 ppm NH_3 showed a response value of 5% at room temperature, whereas the other two samples exhibited much higher values towards similar condition NH_3 at room temperature. Samples with nanowires showed a three-fold increase and samples with nanoparticles exhibit a two-fold increase in response value. We have found that the response of all samples increases with elevating the operating temperature up to 200°C. Increasing the operating temperature improved the nanoparticle sensing conditions more than the other two samples. The samples using nanoparticles showed a 33% increase in response towards 50 ppm NH_3 at 200°C compared to the samples with thin films at similar conditions. Further, response and recovery time were investigated and reported in this study.

Introduction

There is a vast investigation in the literature for gas sensor materials including semiconductor [1], Metal Oxide-Based [2], Nano fibers [3], Carbon-Based [4]. However, there is a lack of information for NH_3 sensing using different TiO_2 nanostructures.

Nanostructured Materials, having the size in the range from 1 nm to 100 nm, showing amazing properties that differ from conventional materials [5]. In gas sensor field, porosity and a high surface-to-volume ratio in order to emphasize surface effects are essential to obtain the properties appropriate for gas-sensing applications [1, 6-7]. The two properties play a more important role in nanostructure materials [8]. In addition, the electrical properties of such nanostructured materials on a high aspect ratio may be easily changed in the presence of small amounts of gas molecules [9].

Semiconductor metal oxide (SMO) gas sensors are the most popular because of quick and precise responses [1, 10]. TiO_2 has a wide range of applications as gas sensors in a medical controller and particular environment [11, 12]. Improvements in gas sensing parameters have been reported in various titanium Nano-structures [13]. In Nano-structure sensors, drift, molecular, and surface mechanisms which are reported very commonly, make them more sensitive adequate at room temperature [14, 15].

The change in conductivity in metal oxide gas sensors such as Titanium dioxide (TiO_2) is due to two factors: the change in carrier density or the change in bending of the energy band structure in the presence of gas [16]. The sensor mechanism of the bulk TiO_2 has been modeled in various forms [17-21]. Generally, in a non-porous structure, gas molecules are decomposed by physical absorption followed by

chemical reaction with oxygen atoms on the semiconductor surface. The result of this interaction with the surface reduces oxygen and thus increasing the number of free electrons in the oxide body [22].

It was shown that the sensing property of TiO_2 similar to semiconductor material increases as the size of the grains decreases [23]. On the strength of this consideration nanostructured TiO_2 can be a good candidate for gas sensors.

Due to the reduction of grain size TiO_2, the sensitive layer allows high surface-volume ratio and results in a high level of sensitivity and selectivity [1, 24].

Ammonia with the formula NH_3, the most important hydrogenated compound in nitrogen, is naturally derived from the decomposition of nitrogenous organic matter [25, 26]. It is a colorless gas with an extremely nasty taste that is also tearful and suffocating [27]. Therefore, it is important to detect a very small volume of this gas in the industry.

In this paper, three different structures of TiO_2 nanostructures used as an ammonia gas sensor at room temperature (25 °C) are examined: I. Thin film II. Nanowire III. Nanoparticles. Different methods of synthesis and characterization to optimize the growth process are examined and tested. The measurement methods were applied to all the three structures.

Experimental

A. Growth of TiO_2 Nanoparticles by Sol-Gel Method

Different sol-gel methods for synthesis have been proposed including [28, 29]. It has been reported that different phases of the formation of anatase and rutile are the result of different growth methods [30]. In this study, TiO_2 was synthesized by the sol-gel method in various alcohol solvents [31]. It should be noted that the Changes in photocatalytic properties, thermal stability, electrical properties and nanoparticle dimensions are the result of these variations synthesis.

In this study, two different solvents were used for the growth of titanium dioxide nanoparticles by sol-gel method, 0.75 milliliters of Titanium isopropoxide ($Ti\{OCH(CH_3)_2\}_4$) were dissolved in 1.5 milliliter alcohol and 1.5 milliliter Acetic acid (CH_3COOH) solution by continuous magnetic stirring for 30 minutes as well as 0.3 grams of Polyvinylpyrrolidone ($\{C_6H_9NO\}$ n) were dissolved in Alcoholic solvent in similar situations. The two solvents were mixed for 120 minutes. Finally, the mixture was deposited on the quartz substrate by spin coating. To complete the growth processes the sample was placed in the oven at a temperature of 450 °C for one hour. The final thickness of the sample was measured as 100 nm. The morphology and microstructure of nanoparticles of titanium dioxide were examined by SEM. As shown in the Fig. 1 the film exhibit structure pore which is important for gas sensing application.

B. Growth of TiO_2 Nanowire by hydrothermal Method

Since nanowire and nanotube of titanium dioxide have a high share of commercial production [32], in various investigations, several methods have been developed for the fabrication of these nanowires, including laser ablation [33], solution–liquid–solid [34], arc discharge [35], vapor–liquid–solid [34], and template-based synthetic approaches [36], which have all been proved to be successful methods for various methods. However, all of the methods used in this study are either physical template or catalyst materials, which may cause contamination in the samples. Therefore, it is believed to use a hydrothermal synthesis nanowire without using preformed templates or catalyst materials [37]. Therefore, the growth of titanium dioxide nanowires by a hydrothermal method is one of the attractive and widely used methods. In this study the growth of nanowires, TiO_2 has been performed using 0.3 molar Titanium isopropoxide were mixed with 0.1 molar Ethanolamine in a magnetic stirrer for 2 hours. Further 10 molar Sodium hydroxide (NaOH) was dropped into the mixture and it was put back on the magnetic stirrer for one hour. The resulting solution was held for 20 hours at 150 °C. After this period, the solution was returned to room temperature naturally. Obtained sediment was centrifuged and washed several times with distilled water and was put at 60 °C to dry for 24 hours. Dried sediment was collected and put in 0.1 molars hydrochloric acid (HCL) solution for one hour. The white color sediment was collected by centrifugation and washed several times again with distilled water and ethanol (C_2H_6O) and dried at 100 °C for one hour. Finally, nanowire titanium dioxide was obtained by baking sediment at 500 °C in air for another hour. Fig. 2 shows the SEM micrograph of the sample grown with the method mention above.

C. Growth of TiO_2 thin-film by sputtering Method

In this method, The TiO_2 Nano composite was fully grown by RF sputtering technique on the quartz substrate. To prepare Target, ten grams of TiO_2 powder was mixed with polyvinyl alcohol ($[CH_2CH(OH)]n$). The mixture was baked at 1000 °C. Sputtering is performed at a vacuum pressure of 2.5 mTorr and a surface temperature of approximately 200 °C. RF power, base pressure and argon flow rate have been optimized to 500(W), 1.33×10^{-5}(Pa) and 30 (sccm) respectively. As the sputtering time changes, the thickness of the TiO_2 layer changes from 10 to 100 nm. To crystalline, the TiO_2 thin films of varying thickness were exposed to oxygen at 600 °C. Fig. 3 shows two samples of SEM micrographs of titanium dioxide by the sputtering method with varying thicknesses. In this study, we used sputtered TiO_2 film with 20 nm thickness.

D. Sensing Measurements

For fabrication gas sensor devices the TiO_2 samples were fabricated in 1×1 cm dimensions. Growth processes for each synthesis sample were adjusted to be about 20 nm in thickness for all three samples in the present study.

For electrical contact, the Gold (Au) electrode was deposited using sputtering. The Au thickness was set to 50 nm. Silver paint was used to connect the sample to the measuring circuit. The electrical response of the TiO_2 was tested toward several ppm NH_3 at room temperature. According to the generally acknowledged definition [38], the response of a sensor to a given concentration [gas] of an oxidizing/reducing, gas is:

$$response = \frac{|R_{gas} - R_{air}|}{R_{air}} \cdot \frac{1}{[gas]} \quad (1)$$

R_{air} is the resistance of two ends of the terminal before gas exposure in stable mode and R_{gas} is exact resistance after gas exposure. We set the [gas] for 50 ppm, 100 ppm and 200 ppm one, two and four respectively.

The measured resistance (R_{air}) for thin-film, nanoparticle and nanowire are 0.45M, 1.1M and 0.54M ohm, respectively.

Ammonia gas is prepared by heating a mixture of ammonium chloride and slaked lime in the ratio of 2 : 3 by mass and passing the gas through the drierite. Moist ammonia gas is dried over quilklime (CaO). Nitrogen (N_2) gas flow was used to control the concentration of ammonia gas. N_2 gas was flowing into the gas chamber up to the system reached a steady-state situation. The concentration of ammonia gas has been determined by the ratio of the flow rate of ammonia and nitrogen gases entering to the chamber.

Results And Discussion

A. Structure characterization

Fourier-transform infrared spectroscopy (FTIR) and X-ray diffraction (XRD) were used to characterize three Nano-structure samples.

FTIR (JASCO, model: 460 Plus) studies of the TiO_2 grown in all three structures showed the characteristics of the formation of high purity product with the least amount of impurity. Fig. 4 shows a sequence of FTIR spectra for TiO_2 nanowire, nanoparticle and thin-film in the range of 500–4000 cm^{-1}. As reported in the literature [39] the peaks at 3440 cm^{-1} in the spectra are due to the stretching and bending vibration of the -OH group. The peaks at 1620 cm^{-1} show stretching vibrations of Ti-O-Ti. Further, the peak observed at 690 cm^{-1} is due to the vibration of the Ti-O-O bond. Therefore, it is obvious that The FTIR spectra clearly exhibit the presence of Ti-O bonds in all the three samples.

Moreover, XRD (Inel, model: EQUINOX3000) was conducted to determine the phase analysis of each sample. In our XRD equipment monochromatic optic Kα1 or Kα1/2 were used. Fig. 5 presents the XRD pattern of the synthesized samples where the peaks of anatase and rutile nanoparticles are well

recognized. As shown in Fig. 5 both nanoparticle and nanowire samples show only the anatase phases, but the rutile phase is observed only in a thin-film sample. XRD pattern specifies the phases and sizes of crystalline materials, providing a determination of the ratio of the anatase phase to the rutile phase in the TiO_2 Nano-structures. Three peaks were considered for the study, and using the Debye- Scherer formula, the grain size was calculated for all three peaks. From Fig. 5, considering the peak Full Width at Half Maximum (FWHM), the average particle size is calculated. This size was calculated for nanowire and nanoparticles samples less than 100 nm while for thin-film sample more than 100 nm was obtained. Peaks in XRD pattern at 2θ=25° (101) and 2θ=48° (101) indicated the presence of the anatase phase while peaks at 2θ=27.5° (110) demonstrated the occurrence of rutile phase. All three peaks suggest that the prepared samples are in a hexagonal structure. The pattern matches well with the standard JCPDS files # 21-12729 [40]. The intensity of XRD peaks of the nanowire and Nano-particle TiO_2 samples shows that the formed nanoparticles are crystalline and broad diffraction peaks indicate small size crystallite. Since in the present study, the sensors were tested at room temperature, there is no concern about the phase change.

B. Electrical measurement

Gas sensing measurements have been conducted under constant temperature conditions at room temperature with different ammonia concentrations.

For measurements and tests of TiO_2 samples the circuit shown in Fig. 6 is used. The silver paint was used to connect the external contact to Au electrodes. The electrical characteristics of the TiO_2 sensors were obtained from the I-V curve of the electrodes junction measured by the KEITHLEY 228A voltage/current source and Sanwa PC7000 Handheld multimeter. To dynamic gas sensing measurements in this investigation, studied devices were placed in a chamber with a continuously gas flow. The humidity control was performed using silica gel. Besides, temperature and humidity sensors are placed in the sensing chamber for online monitoring.

In the first step, the response of the samples toward the different amounts of NH_3 gas has been measured. As shown in Fig. 7 the highest response was observed in the nanowire TiO_2 sample toward different concentrations. The response to ammonia gas in the nanoparticle TiO_2 was very close to the response of the nanowire sample, but the response of the thin-film TiO_2 sample was approximately half that of the nanowire TiO_2 sample. As shown in the SEM pictures (Fig. 1 and Fig. 2) in the nanowire and nanoparticle samples with high porosity, a larger surface-to-volume ratio is seen because the surface arrangement of atoms is slightly different from that of the body [41] and so surface oxygen molecules are easily removed from the surface and create oxygen vacancies [40]. Further, as it is shown in Fig. 7 when the inlet NH_3 gas concentration increased, the response also increased in all three samples. At a high concentration of 200 ppm, the percentage of response differences between the thin-film sample and the other two samples was less compare to lower NH_3 concentration. This phenomenon implies that at

higher concentrations of gas, other defects such as interstitial ions Ti^{3+} and Ti^{4+} in the titanium dioxide lattice play a role in the gas sensing mechanism [42]. The amount of oxygen vacancies in the TiO_2 at the room temperature is not sufficient for gas sensing. But, in Nano-structure TiO_2, due to the presence of a very large volume to surface ratio, there is a lot of surface oxygen with dangling bonds, which can be absorbed by ammonia molecules and extracted from TiO_2. This process can lead to the release of carriers in titanium dioxide and thus, a change in the Fermi level. When surface of Nano-structures TiO_2 is exposed to gas molecules, the oxyanions react with the ammonia molecules and deliver a large number of carries to the grains [43]. In a non-porous structure, gas molecules react by physically and then chemically adsorbed on the oxide semiconductor surface, decomposed by semiconductor oxygen atoms. The result of this surface interaction is the reduction of oxygen, resulting in an increase in the number of free electrons in the oxide body, which increases conductivity [44]. In the polycrystalline structure, the determining factor for the conduction of the sensitive layer is the potential barrier height between the grains. At the grain level, oxygen can be absorbed to the grain surface in forms of O^{2-}, O^{-} and O_2^{-} creating a potential barrier at the grain boundaries. So typically, the semiconductor oxide sensor properties increase with decreasing grain size [23]. Therefore, nanowire and nanoparticle samples that have smaller grain size boundaries will show higher response.

The change in conductivity in metal oxide gas sensors is due to two factors: change the carrier density or bending of energy bands in the presence of gas [1]. The speed of carrier response or bending change was examined after applying the gas to the surface. Fig. 8 shows response and recovery times after inserting the NH_3 gas and disconnecting the flow of the gas. Response time for the nanowire and nanoparticle samples have been recorded around 40 seconds while for thin-film sample showed a response time of around 70 seconds. Recovery times in three samples were measured approximately 15 seconds. As discussed earlier the nanowire and nanoparticle films exhibited more pores than thin films. So due to the greater porosity of the nanowire and the nanoparticle samples, the number of molecules reaching the surface increase and create lower Response Times. However, porosity does not have much effect on recovery time.

In the nanocrystals, the interaction of the gas molecules with other molecules like water molecules adsorbed on the surface of the grains has a greater effect on the electrical conductivity of the sensitive layer [22]. The change in the number of atoms absorbed at the surface controls the mobility of the carriers by changing the number of distributed carriers [45]. The presence of water molecules can interfere with the gas molecules absorbed on the surface. Two different tests were performed to accurately examine the effect of humidity.

First, the fabricated sensors considered as the humidity sensor. Humidity sensing was performed at room temperature and 760 mmHg pressure. As shown in Fig. 9 (a) the response of the samples to humidity is very low compared to ammonia gas. All three sensors showed a very small response to change in relative humidity. Most sensitivities observed for thin-film, nanoparticle and nanowire were 0.019, 0.035 and 0.034, respectively at 80% relative humidity. In this experiment dry environment is considered below 10%

relative humidity and concentration [gas] in the response equation (1) for 80% relative humidity was equal to 50 ppm. Since the response of samples is very low in the presence of different humidity, these samples cannot be a humidity sensor.

In the second experiment, changes in humidity during ammonia gas sensing were investigated. Fig. 9(b) shows the changes in the response of the different samples versus humidity. The response values have been obtained from the results shown in Fig. 7. As shown in Fig. 9(b) the response decrease slightly with increasing humidity up to 60%. Though the response decreases drastically above 60% of humidity's.

As shown in Fig. 9(b) humidity effect toward 50 ppm NH_3 gas response is less than 3% up to 60% relative humidity for samples. Also the sensor response to 10-90 relative humidity has experimented for all three samples.

To characterize the response of the three sensors at the higher operating temperature we measured the senility of the samples at various temperatures from 25 °C to 200 °C. As reported in the literature [42] the sensing mechanism TiO_2 change with temperature. These can be due to the different oxygen densities in TiO_2 with various temperatures. It is believed that higher temperatures create lattice defects in TiO_2 [46]. Oxygen vacancies at higher temperatures diffused rapidly with high mobility into the TiO_2 body as so these define the conductivity of TiO_2 sensors [47]. As Fig. 10 illustrates, increasing the temperature to around 200 °C resulted in a significant increase in response. This increase was observed more than 3.5 times in the nanoparticle sample compared to the sample operated at room temperature. Further, the effect of temperature on the response of the nanoparticle sample was greater than that of the nanowire sensor. The difference is because the nanoparticle sample has a higher porosity than the other films increasing the properties of the body O_2 in the sensing mechanism.

To consider the thermal and electrical stability of the fabricated samples, two tests were performed without inserting gas into the test chamber: First, we applied a voltage of 40V DC for 24 hours [48] followed by testing the samples in an oven at 400 °C for 8 hours [1]. After the tests, samples left over for three months under normal room conditions. Gas sensing tests were performed on the samples again. As shown in Fig. 11 the results showed that the nanowire sample was more stable than the other samples. Significant differences were observed in the response of the nanoparticle and thin-film in the response time and the recovery time for the fabricated samples and those tested after three months. Condition 1 shows the results of the response just after the fabrication of TiO_2 and using Condition 2 exhibits the results obtained after 3 months.

Conclusion

In this study, three different structures of titanium dioxide Nano-structure of a nanowire, nanoparticle and thin-film were fabricated for ammonia gas sensing applications. The growth of the nanowire, nanoparticle and thin-film of TiO_2 structures have been conducted on quartz glasses using hydrothermal, sol-gel and RF sputtering, respectively. The structures of the fabricated samples were examined by SEM

micrograph, FTIR characterization and XRD pattern and so the correct growth and formation of the TiO_2 lattice were confirmed. From the results obtained in this study, we may conclude that the nanowire samples operated at room temperature exhibit more sensing response toward low NH_3 conditions. Moreover, higher electrical and thermal stability were also compared to the other two samples. Finally, we confirmed the nanowire samples indicate a much higher response and stability than the other two sensors.

References

1. A. Dey, "Semiconductor metal oxide gas sensors: A review". Materials Science and Engineering: B vol. **229**, 206–217 (2018)
2. M. Hadiyan, A. Salehi, *and* A. Koohi-Saadi, "Sub-ppm acetone gas sensing properties of free-standing ZnO nanorods" Journal of Electroceramics, *pp.* 1–9, 2019
3. C. De Pascali, M. A. Signore, A. Taurino, L. Francioso, A. Macagnano, J. Avossa, *et al.*, "Investigation of the Gas-Sensing Performance of Electrospun TiO 2 Nanofiber-Based Sensors for Ethanol Sensing" IEEE Sens. J., *vol.* 18, 7365–7374, 2018
4. M. Shooshtari, A. Salehi, *and* S. Vollebregt, Effect of Humidity on Gas Sensing Performance of Carbon Nanotube Gas Sensors Operated at Room Temperature IEEE Sens. J., 21, 5763–5770, 2020
5. J. Zhang, X. Liu, G. Neri, *and* N. Pinna, "Nanostructured materials for room-temperature gas sensors," Advanced materials, *vol.* 28, *pp.* 795–831, 2016
6. M.-H. Seo, M. Yuasa, T. Kida, J.-S. Huh, K. Shimanoe, *and* N. Yamazoe, "Gas sensing characteristics and porosity control of nanostructured films composed of TiO2 nanotubes," Sensors and Actuators B: Chemical, *vol.* 137, *pp.* 513–520, 2009.
7. A. Salehi, D. J. Kalantari, *and* A. Goshtasbi, *"Rapid response of Au/porous-GaAs humidity sensor at room temperature," in* 2006 *Conference on Optoelectronic and Microelectronic Materials and Devices, 2006, pp. 125–128.*
8. V. Galstyan, E. Comini, C. Baratto, G. Faglia, *and* G. Sberveglieri, "Nanostructured ZnO chemical gas sensors," Ceramics International, *vol.* 41, 14239–14244, 2015
9. B. Yuliarto, L. Nulhakim, M.F. Ramadhani, M. Iqbal, *and* A. Nuruddin, Improved performances of ethanol sensor fabricated on Al-doped ZnO nanosheet thin films IEEE Sens. J., *vol.* 15, 4114–4120, 2015
10. P.T. Moseley, Progress in the development of semiconducting metal oxide gas sensors: a review. Meas. Sci. Technol. vol. **28**, 082001 (2017)
11. Aoboun, A., Cherdhirunkorn, B. & Pechyen, C. Development of screen printed electrode using MWCNTs–TiO2 nanocomposite as a low-cost device for uric acid detection in urine. J Mater Sci: Mater Electron 30, 2403–2412, 2019.
12. S. Sakib, R. Pandey, L. Soleymani, *and* I. Zhitomirsky, Surface modification of TiO2 for photoelectrochemical DNA biosensors Medical Devices & Sensors, *vol.* 3, e10066, 2020

13. S. Wategaonkar, R. Pawar, V. Parale, D. Nade, B. Sargar, *and* R. Mane, *"Synthesis of rutile TiO2 nanostructures by single step hydrothermal route and its characterization," Materials Today: Proceedings, vol. 23, pp. 444–451*, 2020
14. I. Cappelli, A. Fort, A. Lo Grasso, E. Panzardi, M. Mugnaini, *and* V. Vignoli, "RH Sensing by Means of TiO2 Nanoparticles: A Comparison among Different Sensing Techniques Based on Modeling and Chemical/Physical Interpretation," Chemosensors, *vol.* 8, *p.* 89, 2020
15. Karthik, P., Gowthaman, P., Venkatachalam, M. et al. Propose of high performance resistive type H2S and CO2 gas sensing response of reduced graphene oxide/titanium oxide (rGO/TiO2) hybrid sensors. J Mater Sci: Mater Electron 31, 3695–3705, 2020.
16. V. Ganbavle, S. Inamdar, G. Agawane, J. Kim, *and* K. Rajpure, "Synthesis of fast response, highly sensitive and selective Ni: ZnO based NO2 sensor," Chemical Engineering Journal, *vol.* 286, *pp.* 36–47, 2016.
17. X. Chen and A. Selloni, *"Introduction: titanium dioxide (TiO2) nanomaterials," ed: ACS Publications*, 2014.
18. B. Comert, N. Akin, M. Donmez, S. Saglam, *and* S. Ozcelik, Titanium dioxide thin films as methane gas sensors IEEE Sens. J., *vol.* 16, 8890–8896, 2016
19. E. Bet-Moushoul, Y. Mansourpanah, K. Farhadi, *and* M. Tabatabaei, "TiO2 nanocomposite based polymeric membranes: a review on performance improvement for various applications in chemical engineering processes," Chemical Engineering Journal, *vol.* 283, *pp.* 29–46, 2016.
20. Z. Li, Z. Yao, A. A. Haidry, T. Plecenik, L. Xie, L. Sun, *et al.*, "Resistive-type hydrogen gas sensor based on TiO2: a review," International Journal of Hydrogen Energy, 2018.
21. O. Krško, T. Plecenik, T. Roch, B. Grančič, L. Satrapinskyy, M. Truchlý, *et al.*, "Flexible highly sensitive hydrogen gas sensor based on a TiO2 thin film on polyimide foil," Sensors and Actuators B: Chemical, *vol.* 240, *pp.* 1058–1065, 2017.
22. X. Zhou, Y. Wang, J. Wang, Z. Xie, X. Wu, N. Han, *et al.*, "Amplifying the signal of metal oxide gas sensors for low concentration gas detection" IEEE Sens. J., *vol.* 17, 2841–2847, 2017
23. B. Lyson-Sypien, M. Radecka, M. Rekas, K. Swierczek, K. Michalow-Mauke, T. Graule, *et al., "*Grain-size-dependent gas-sensing properties of TiO2 nanomaterials," Sensors and Actuators B: Chemical, *vol.* 211, *pp.* 67–76, 2015.
24. G. Eranna, B. Joshi, D. Runthala, *and* R. Gupta, Oxide materials for development of integrated gas sensors—a comprehensive review Crit. Rev. Solid State Mater. Sci., *vol.* 29, 111–188, 2004
25. H. Wu, Z. Ma, Z. Lin, H. Song, S. Yan, *and* Y. Shi, "High-sensitive ammonia sensors based on tin monoxide nanoshells," Nanomaterials, *vol.* 9, *p.* 388, 2019
26. M. Hakimi, A. Salehi, F. Boroumand, *and* N. Mosleh, Fabrication of a room temperature ammonia gas sensor based on polyaniline with N-doped graphene quantum dots IEEE Sens. J., *vol.* 18, 2245–2252, 2018
27. J.N. Gavgani, A. Hasani, M. Nouri, M. Mahyari, *and* A. Salehi, Highly sensitive and flexible ammonia sensor based on S and N co-doped graphene quantum dots/polyaniline hybrid at room temperature

Sens. Actuators B, *vol.* 229, 239–248, 2016

28. S. S. Al-Taweel and H. R. Saud, "New route for synthesis of pure anatase TiO2 nanoparticles via ultrasound assisted sol-gel method," Journal of Chemical and Pharmaceutical Research, *vol.* 8, *pp.* 620–626, 2016.
29. R. Nankya and K.-N. Kim, "Sol–Gel Synthesis and Characterization of Cu–TiO2 Nanoparticles with Enhanced Optical and Photocatalytic Properties," Journal of Nanoscience and Nanotechnology, *vol.* 16, *pp.* 11631–11634, 2016.
30. B. K. Mutuma, G. N. Shao, W. D. Kim, *and* H. T. Kim, "Sol–gel synthesis of mesoporous anatase–brookite and anatase–brookite–rutile TiO2 nanoparticles and their photocatalytic properties," Journal of colloid and interface science, *vol.* 442, *pp.* 1–7, 2015.
31. O. Wiranwetchayan, S. Promnopas, T. Thongtem, A. Chaipanich, *and* S. Thongtem, "Effect of alcohol solvents on TiO2 films prepared by sol–gel method," Surface and Coatings Technology, *vol.* 326, *pp.* 310–315, 2017.
32. D. V. Bavykin, J. M. Friedrich, *and* F. C. Walsh, "Protonated titanates and TiO2 nanostructured materials: synthesis, properties, and applications," Advanced Materials, *vol.* 18, *pp.* 2807–2824, 2006.
33. P. Liu, W. Cai, M. Fang, Z. Li, H. Zeng, J. Hu, *et al.*, "Room temperature synthesized rutile TiO2 nanoparticles induced by laser ablation in liquid and their photocatalytic activity," Nanotechnology, *vol.* 20, *p.* 285707, 2009.
34. Y. Wu, P. Yang, Direct observation of vapor – liquid – solid nanowire growth. J. Am. Chem. Soc. vol. **123**, 3165–3166 (2001)
35. S. K. Pradhan, P. J. Reucroft, F. Yang, *and* A. Dozier, "Growth of TiO2 nanorods by metalorganic chemical vapor deposition," Journal of Crystal Growth, *vol.* 256, *pp.* 83–88, 2003.
36. H. Shang, G. Cao, *"Template-based synthesis of nanorod or nanowire arrays," Springer Handbook of Nanotechnology, pp. 161–178*, 2007
37. M. Ge, J. Cai, J. Iocozzia, C. Cao, J. Huang, X. Zhang, *et al.*, "A review of TiO2 nanostructured catalysts for sustainable H2 generation," international journal of hydrogen energy, *vol.* 42, *pp.* 8418–8449, 2017.
38. M. Ferroni, V. Guidi, G. Martinelli, G. Faglia, P. Nelli, *and* G. Sberveglieri, "Characterization of a nanosized TiO2 gas sensor," Nanostructured materials, *vol.* 7, *pp.* 709–718, 1996.
39. A. León, P. Reuquen, C. Garín, R. Segura, P. Vargas, P. Zapata, *et al.*, "FTIR and Raman characterization of TiO2 nanoparticles coated with polyethylene glycol as carrier for 2-methoxyestradiol," Applied Sciences, *vol.* 7, *p.* 49, 2017.
40. H. Ijadpanah-Saravy, M. Safari, A. Khodadadi-Darban, *and* A. Rezaei, Synthesis of titanium dioxide nanoparticles for photocatalytic degradation of cyanide in wastewater Anal. Lett., *vol.* 47, 1772–1782, 2014
41. Y. Kwon, H. Kim, S. Lee, I.-J. Chin, T.-Y. Seong, W. I. Lee, *et al.*, "Enhanced ethanol sensing properties of TiO2 nanotube sensors," Sensors and Actuators B: Chemical, *vol.* 173, *pp.* 441–446, 2012.

42. L. Xu, X. Ma, N. Sun, *and* F. Chen, "Bulk oxygen vacancies enriched TiO2 and its enhanced visible photocatalytic performance," Applied Surface Science, *vol.* 441, *pp.* 150–155, 2018.
43. S. Ramanavicius, A. Ramanavicius, "Insights in the Application of Stoichiometric and Non-Stoichiometric Titanium Oxides for the Design of Sensors for the Determination of Gases and VOCs (TiO2 – x and TinO2n – 1 vs. TiO2)," Sensors, *vol.* 20, *p.* 6833, 2020
44. P. Gwizdz, M. Radecka, *and* K. Zakrzewska, *"Array of Gas Sensors Based on TiO2 upon Temperature Modulation," in 2018 XV International Scientific Conference on Optoelectronic and Electronic Sensors (COE)*, 2018, *pp. 1–4.*
45. C.-H. Lin, C.-H. Liao, W.-H. Chen, C.-Y. Chou and C.-Y. Liu, "Fabrication of p-type TiO2 and transparent p-TiO2/n-ITO pn junctions," AIP Advances, *vol.* 9, *p.* 045229, 2019.
46. S. Lin, D. Li, J. Wu, X. Li, *and* S. Akbar, "A selective room temperature formaldehyde gas sensor using TiO2 nanotube arrays," Sensors and Actuators B: Chemical, *vol.* 156, *pp.* 505–509, 2011.
47. W. Wang, F. Liu, B. Wang, *and* Y. Wang, "Effect of defects in TiO2 nanoplates with exposed {001} facets on the gas sensing properties," Chinese Chemical Letters, *vol.* 30, *pp.* 1261–1265, 2019.
48. M. Tabatabaei, H. G. Fard, *and* J. Koohsorkhi, "Low-Temperature Preparation of a Carbon Nanotube–ZnO Hybrid on Glass Substrate for Field Emission Applications," Nano, *vol.* 10, *p.* 1550040, 2015

Declarations

Declaration of interests-

The authors declare that they have no known competing financial interests or personal relationships that could have appeared to influence the work reported in this paper.

Figures

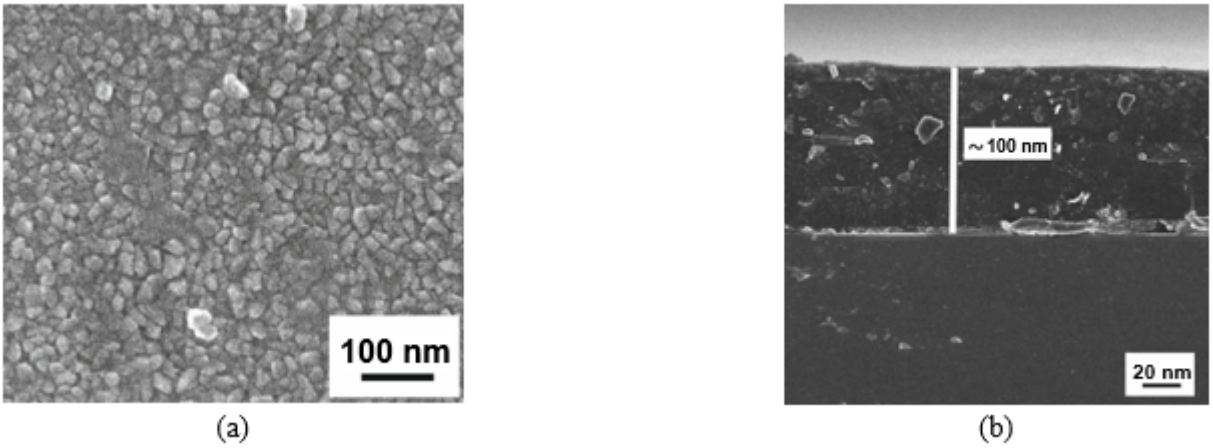

Figure 1

SEM micrograph of titanium dioxide film prepared by sol-gel method a) from top and b) cross section.

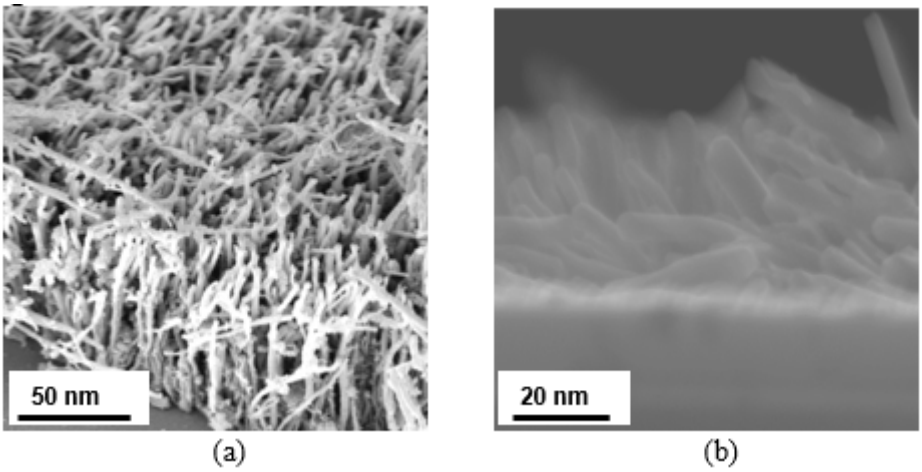

Figure 2

(a) Top view and (b) cross-section SEM micrograph of titanium dioxide film prepared by hydrothermal method.

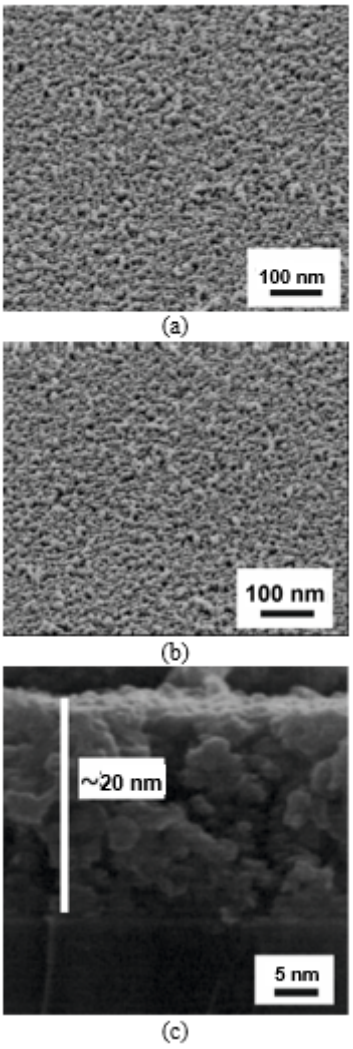

Figure 3

SEM micrograph of titanium dioxide film by a sputtering method with (a) 20 nm thickness from the top, (b) 10 nm thickness from the top and (c) cross-section of TiO2 with 20 nm thickness.

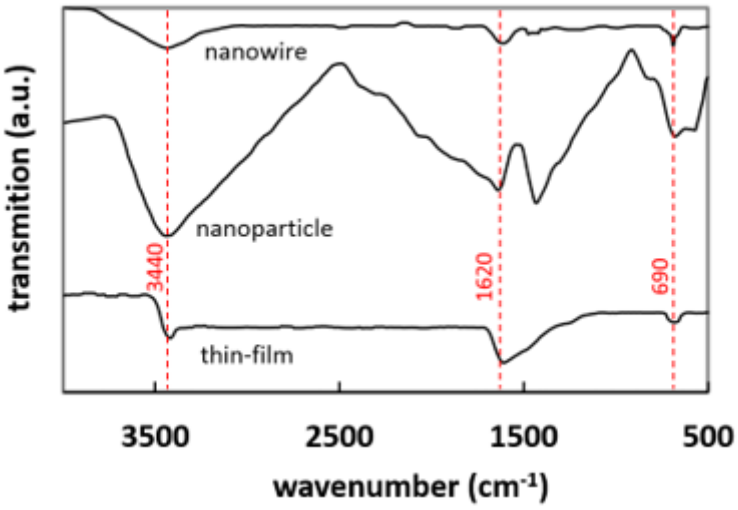

Figure 4

Fourier-transform infrared (FTIR) spectra for three structures of titanium dioxide Nano-structures.

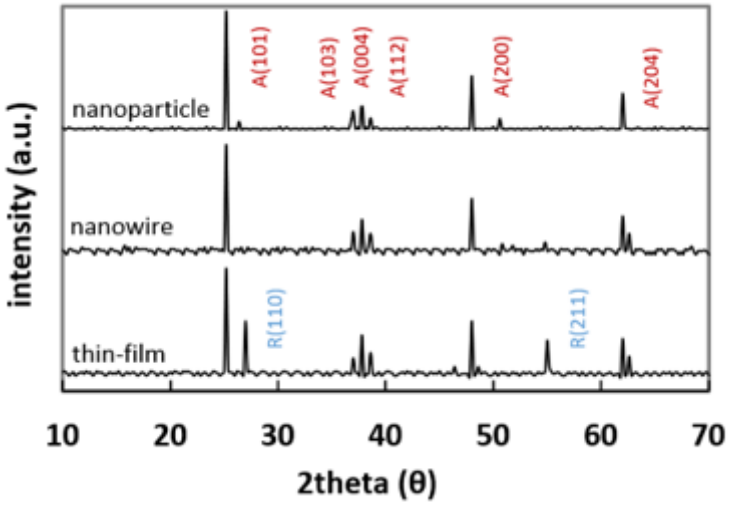

Figure 5

X-ray diffraction (XRD) pattern of synthesized structures for titanium dioxide Nano-structures.

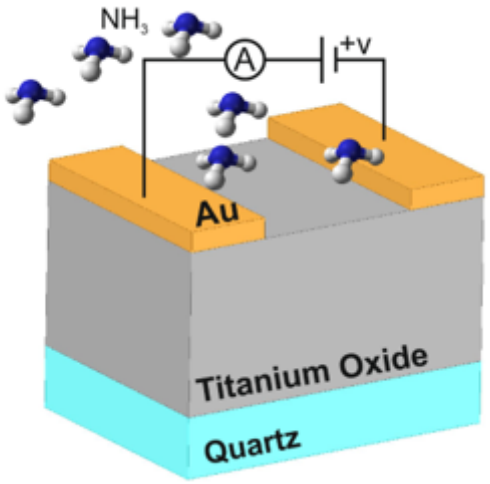

Figure 6

The configuration used for response measurement.

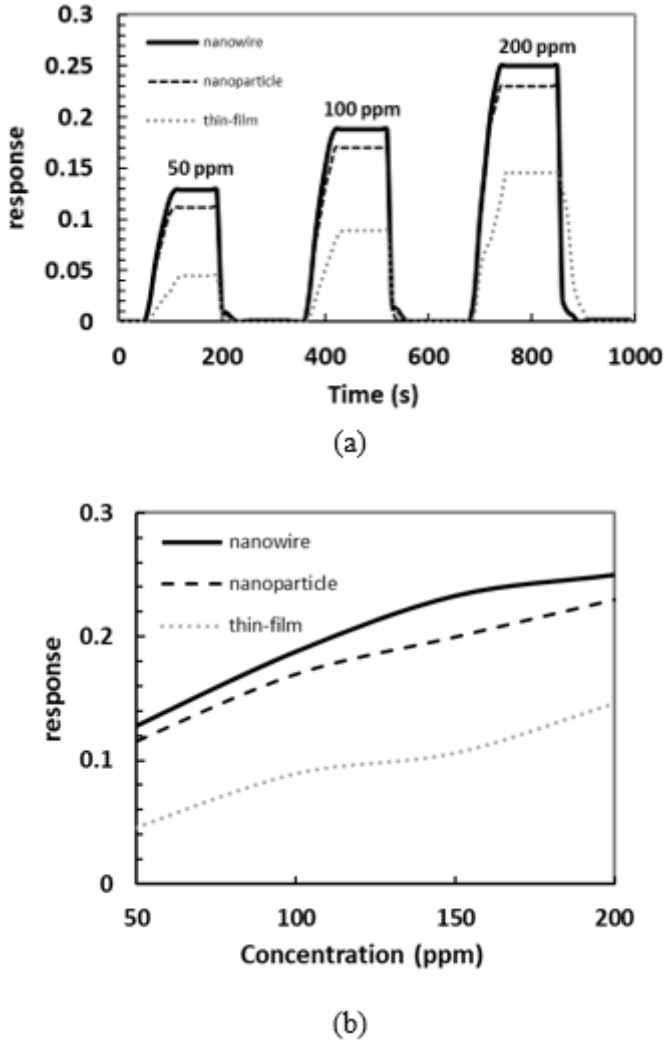

Figure 7

a) Response of nanowire, nanoparticle and thin-film of TiO2 at different concentrations of ammonia gas at room temperature. b) Response vs. ammonia concentration.

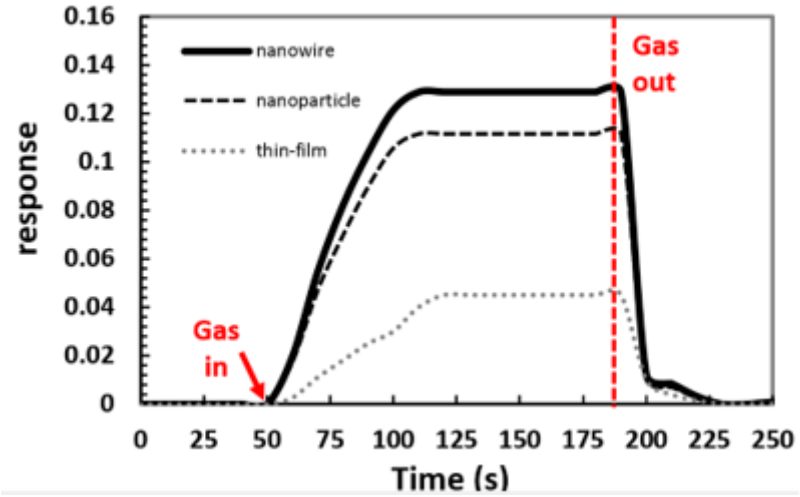

Figure 8

Response of nanowire, nanoparticle and thin-film of TiO2 at 50 ppm concentrations of ammonia gas operated at room temperature.

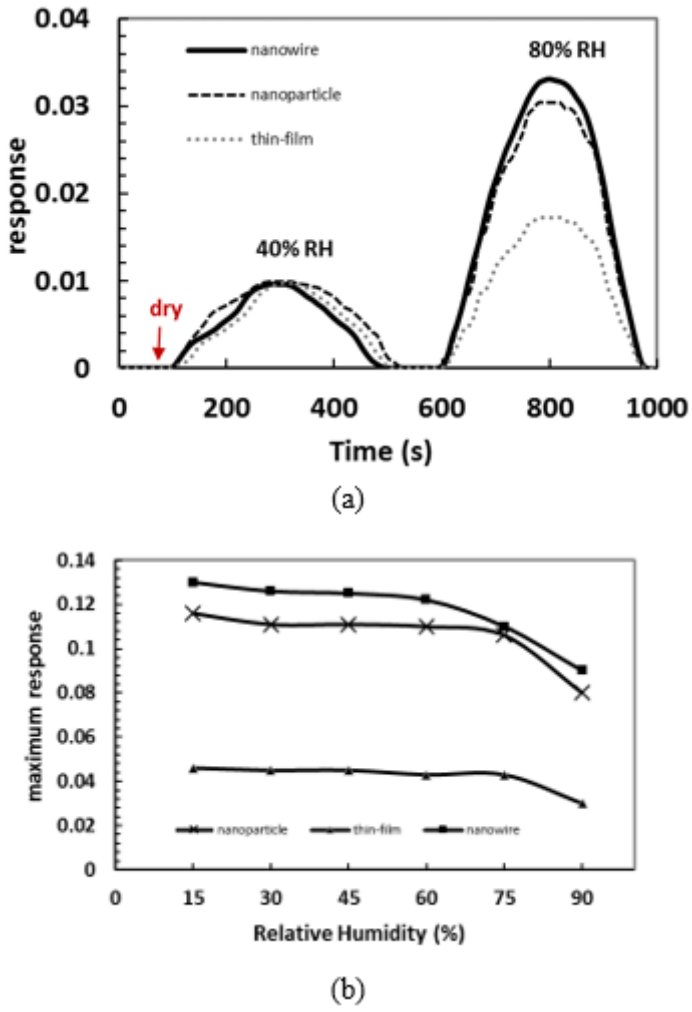

Figure 9

a) The response of nanowire, nanoparticle and thin-film of TiO2 at different relative humidity at room temperature. b) Response vs. relative humidity at 50 ppm concentrations of ammonia gas at room temperature and 760 mmHg.

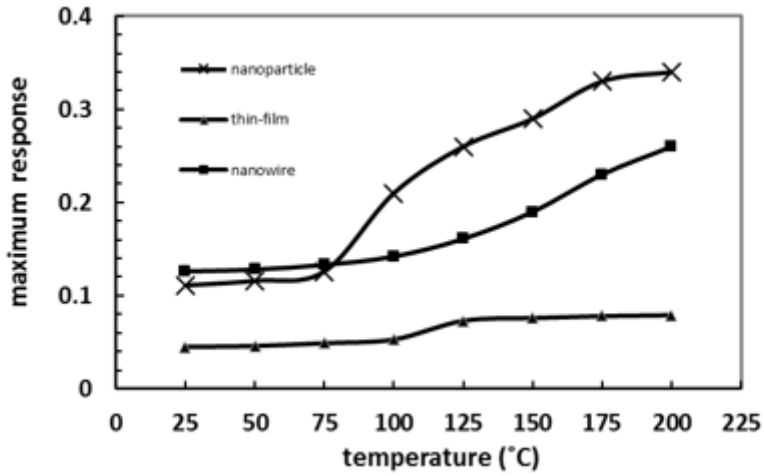

Figure 10

The response of nanowire, nanoparticle and thin-film of TiO2 vs. temperature at 50 ppm concentration of ammonia gas.

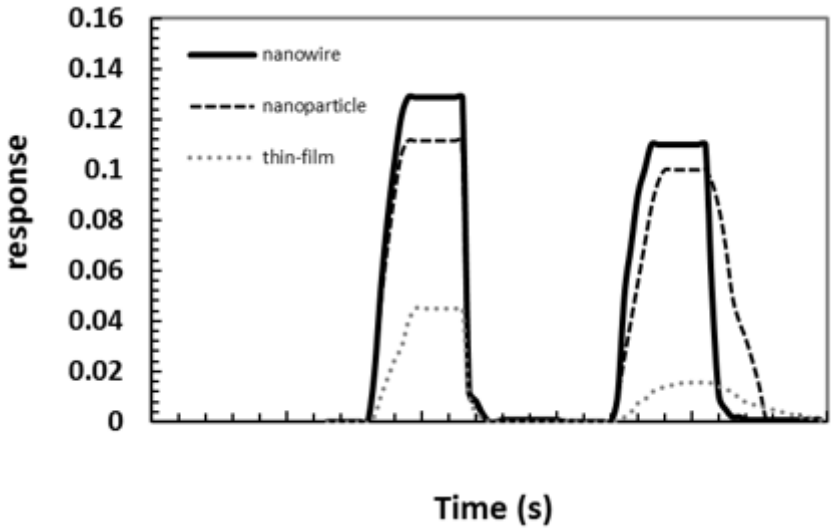

Figure 11

Response of nanowire, nanoparticle and thin-film of TiO2 at 50 ppm concentration of ammonia gas at two different test conditions. Condition 1: Just after sensor fabrication. Condition 2: After 3 months of fabrication and under 40V voltage and 400 °C temperature.